

The detailed mechanism of the η production in pp scattering up to the $T_{lab} = 4.5$ GeV

Saša Ceci,* Alfred Švarc, and Branimir Zauner
Ruđer Bošković Institute,
Bijenička Cesta 54, 10000 Zagreb, Croatia
(Dated: November 5, 2018)

Contrary to very early beliefs, the experimental cross section data for the η production in proton-proton scattering are well described if π and only η meson exchange diagrams are used to calculate the Born term. The inclusion of initial and final state interactions is done in the factorization approximation by using the inverse square of the Jost function. The two body Jost functions are obtained from the S matrices in the low energy effective range approximation. The danger of double counting in the $p\eta$ final state interaction is discussed. It is shown that higher partial waves in meson-nucleon amplitudes do not contribute significantly below excess energy of $Q = 100$ MeV. Known difficulties of reducing the multi resonance model to a single resonance one are illustrated.

PACS numbers: 13.60.Le, 13.75.Cs, 14.40.Ag, 25.40.Ep

I. INTRODUCTION

For a few decades the only way of detecting the η meson signal in the intermediate energy proton-proton scattering was to perform the pionic three-prong experiments and finding the characteristic invariant mass. In the CERN/HERA report [1] a compilation of all mutually normalized and otherwise adjusted experimental data for the $pp \rightarrow pp\eta$ process from $T_{lab} = 2$ GeV to $T_{lab} = 13$ GeV have been presented. Yet, first theoretical models [2, 3, 4] appeared at the beginning of the 90s, accompanied by the first published experimental results [5]. The common denominator of these first models is a similar reaction mechanism: the η meson in two proton collisions is produced when an intermediate meson, emitted in the meson-production vertex, interacts with a proton forming an N^* resonance which decays into η meson and proton. Everything else varies from model to model: the number and type of intermediate mesons (π , η , ρ , ω , σ , ...), the type of excited state (a resonance formation or some re-scattering in addition), etc. The contribution of ρ meson exchange is recognized as a dominant one, or at least of equal importance as the π meson exchange. The influence of η exchange has been considered as insignificant. The higher order terms expressed through different forms of initial and final state interactions had to be included, and it has been shown that they play a crucial role for the reliability of the calculation. The agreement of these models with the experimental data has been obtained by adjusting the free coupling constants. The new measurements have soon appeared [6, 7, 8, 9], and the old models have been improved accordingly [10, 11, 12, 13]. The number and type of exchanged mesons still varied.

A model has been proposed [14] where the meson-nucleon partial-wave T-matrices obtained in the

multi-resonance, coupled channel and unitary model [15] are used in the η -meson production vertex instead of individual N^* resonances. The discussion which intermediate mesons dominate the process is reduced to calculating the $pp \rightarrow pp\eta$ process with the predetermined relative strength of the two-body *eta*-meson production T-matrices for various opened channels. Contrary to former statements, it has been shown that a good agreement with the experimental results for the total cross section is achieved using only π and η contributions, without any need to invoke heavier mesons.

New low energy experiments reporting angular correlation measurements have been done at Jülich [16, 17], so theoretical focus has moved from evaluating total cross section to more detailed calculations [18].

This article offers an improvement of the previous model [14] and the extension of the examined energy range. Basic conclusions of the first model are confirmed: the π and η meson exchange contributions are sufficient for the Born term so there is no demonstrable necessity to introduce other meson contributions; the initial and final state interactions are essential for the shape and size of the cross section. The new, formerly unreachable conclusions presented in this article are enabled by a more transparent treatment of the initial and final state interactions. This model reasonably well describes the total cross section for a wide energy range from very near threshold to $T_{lab} = 4.5$ GeV.

II. FORMALISM

The ingredients of the model are presented in Fig. 1. The differential cross section of the full process is given as:

$$d\sigma = \frac{1}{\mathcal{F}} f_{out} \left| \sum_x \mathcal{E}_{x\eta} \mathcal{P}_x \mathcal{V}_x \right|^2 f_{in} d\Phi \quad (1)$$

*Electronic address: sasa.ceci@irb.hr

where \mathcal{F} is a standard flux factor and $d\Phi$ is the three-body Lorentz invariant phase space. The three-particle vertex \mathcal{V}_x is completely determined by the Bonn potential parameters [19], modified by keeping the momenta in the propagator and form factors relativistic. Pseudoscalar meson-proton coupling constants and cut-off parameters, used in this calculation, are identified with the corresponding on mass shell meson-nucleon values from the same reference: $g_{\pi NN}^2/4\pi = 13.6$, $g_{\eta NN}^2/4\pi = 3$, $\Lambda_\pi = 1.3$ GeV and $\Lambda_\eta = 1.5$ GeV.

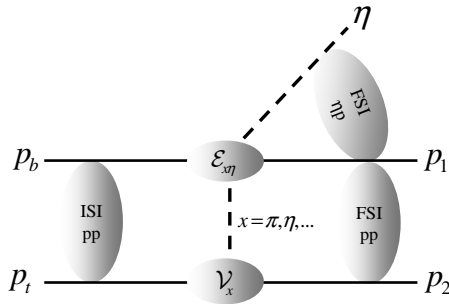


FIG. 1: Ingredients of the model. ISI and FSI represent the initial and final state interactions. \mathcal{V}_x is the Bonn vertex, while the $\mathcal{E}_{x\eta}$ is the η production amplitude.

Eta emission vertex $\mathcal{E}_{x\eta}$ is given by $xp \rightarrow \eta p$ scattering amplitudes from our partial wave analysis [15]. Off-shell amplitudes have been constructed by keeping the multi resonant T -matrices on shell and extrapolating partial wave projectors, following the recipe given in [20].

The initial and final state correction factors have roots in a threshold transition from the initial two proton $^{33}P_1$ state to the final two proton $^{31}S_0$ state with the ηp subsystem in the s-state.

The final state correction factor is given in the factorization approximation using the two body Jost functions in the low energy effective range approximation [21]:

$$f_{out} = \frac{1}{|\mathcal{J}(p_{12})|^2} \frac{1}{|\mathcal{J}(p_{1\eta})\mathcal{J}(p_{2\eta})|^{2n}}, \quad (2)$$

where two body relative momentum is defined as $p_{AB} = |\mathbf{p}_A - \mathbf{p}_B|/2$ with A and B as pairs of the final state particles. The coefficient n is a part of our model. Allowing the possibility that the scattering length a and effective range r are complex numbers, the two body correction factor used for the evaluation of final state contribution - Eq. (2) is, in the s-wave low energy effective range approximation, generically given as:

$$\frac{1}{|\mathcal{J}(p)|^2} = \frac{p^2 - 2p \text{Im} \alpha_+ + |\alpha_+|^2}{p^2 + 2p \text{Im} \alpha_- + |\alpha_-|^2}, \quad (3)$$

where $\alpha_{\pm} = \frac{1}{r} \pm \sqrt{\frac{1}{r^2} + \frac{2}{ar}}$.

To calculate the Jost functions we have used the following pp scattering length and effective range parameters

for the two protons in the $^{31}S_0$ state: $a_0^{pp} = 7.8$ fm and $r_0^{pp} = 2.79$ fm [22].

For the ηp S_{11} subsystem, the s-wave scattering length is given by $a_0^{p\eta} = (0.717 + i 0.265)$ fm [15]. For this article, the corresponding effective range $r_0^{p\eta} = (-1.574 - i 0.020)$ fm has been obtained by fitting the S_{11} wave T -matrix from the same reference.

For the $^{33}P_1$ state, the Jost function has been estimated by using p-wave effective range relation [21]. The used values are $a_{10}^{pp} = -3.3$ fm³ and $r_{10}^{pp} = 4.22$ fm⁻¹ [23].

The initial state factor f_{in} is indistinguishable from unity for energies above η production threshold, while final state correction factor exhibits the distinct variations in magnitude.

III. ASSEMBLING THE MODEL

We have calculated the Born term for this process using the S_{11} meson-nucleon amplitudes of ref. [15] for all three channels: π , η , and the "effective" two body channel. It turns out that the individual contributions of π and η mesons are comparable in size and slightly dominated by the first one. The "effective" meson contribution is negligible [14, 24]. Therefore, from now on the third meson contribution (in which the ρ contribution is implicitly included) will be disregarded in this work.

To determine the relative sign of the remaining two meson contributions, we have to obtain the qualitative and quantitative agreement of the model predicted total cross section with all experimental data available within the low and intermediate energy range. We do it in three steps: we calculate the Born term contribution (model A), add the pp final state interaction (model B), and finally include the $p\eta$ final state interaction. We offer two versions of the $p\eta$ final state interaction: the full Jost function ($n = 1$ in Eq. (2) - model C), and an arbitrary effective reduction of the final state interaction because of possible double counting in the η meson production vertex when the full T -matrices are used instead of individual N^* resonances ($n = \frac{1}{2}$ in Eq. (2) - model D.)

The agreement of the model predictions with the compilation of the experimental data points to the appropriate model.

IV. RESULTS AND CONCLUSIONS

A. Total cross section

The comparison of model predictions with the compilation of experimental cross section data for different π vs. η relative signs is given in Fig. 2 and Fig. 3. The negative π vs. η relative sign, as shown in Fig.2, is ruled out.

The inclusion of the pp final state interaction improves the agreement of the model with the experimental data

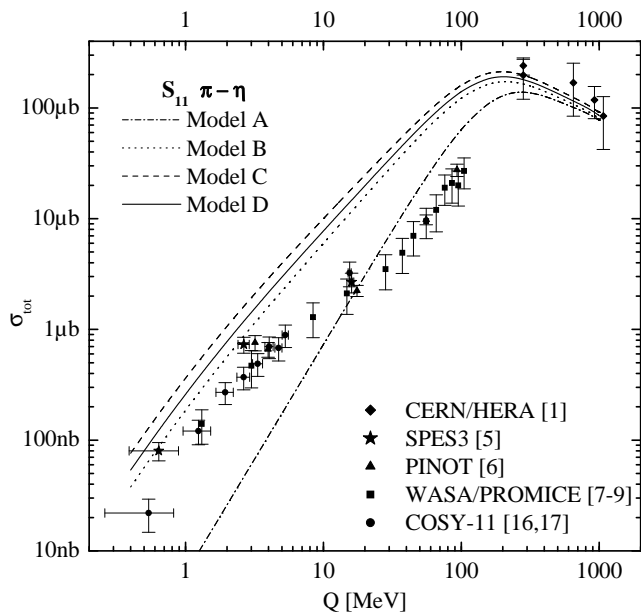


FIG. 2: The total $pp \rightarrow pp\eta$ cross section. S_{11} partial wave in multi resonant model is only used. The negative π vs. η relative sign is chosen. The interference is constructive. Models A,B,C and D are described in the text. Q is the excess energy.

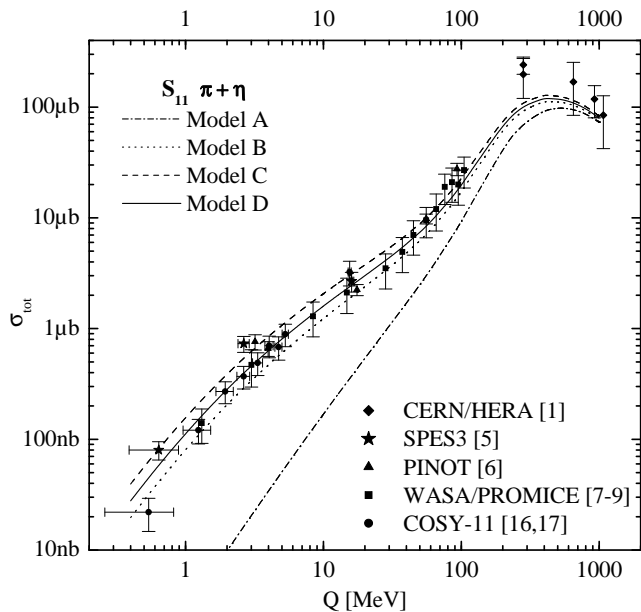


FIG. 3: The total $pp \rightarrow pp\eta$ cross section. S_{11} partial wave in multi resonant model is only used. The positive π vs. η relative sign is chosen. The interference is destructive. Models A,B,C and D are described in the text. Q is the excess energy.

significantly, as can be seen in Fig. 3. Used model for the $p\eta$ FSI gives the overall agreement between the model and experiment (see dashed and full lines in Fig. 3).

Based on the results presented in Fig. 3 we are in favor of model D. However, as the precision of the measured data in the excess energy range of $10 \text{ MeV} < Q < 100 \text{ MeV}$ is not adequate (normalization problems), we can only suspect that the double counting effects are hidden in the proposed formalism.

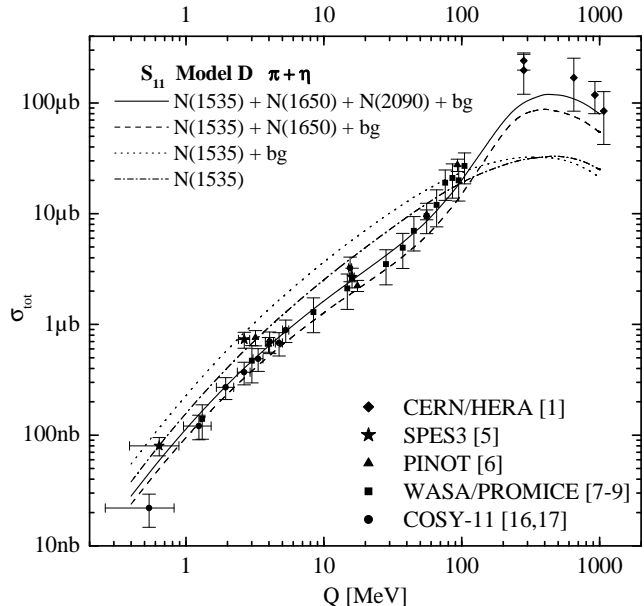


FIG. 4: The total $pp \rightarrow pp\eta$ cross section when individual S_{11} wave resonances are consecutively added to form the two body T -matrix. The resonance nomenclature is taken over from PDG.

The consecutive addition of individual S_{11} wave resonances in forming the partial wave T -matrix is shown in Fig. 4. Results presented in this figure confirm our repeatedly made statement that a single resonance model drastically fails in calculating the total cross section. We find out that *only* the inclusion of *all three* resonances reproduces the measured cross section in the considered energy range.

In Fig. 5 the higher partial-waves are included into the two-body multi resonant T -matrices with the intention of obtaining better agreement with experiment at energies higher than $Q = 100 \text{ MeV}$. The inclusion of higher partial-waves into the πN T -matrices start to be noticeable only at surprisingly high energies (above $Q \approx 300 \text{ MeV}$). That indicates that the improvement of the present model should be directed to a more rigorous treatment of the initial and final state interaction (pp in particular) prior to the possible improvement of the Born term.

Additional experiments in the intermediate energy region ($100 \text{ MeV} < Q < 1 \text{ GeV}$) would be greatly appreciated. Proper ISI and FSI treatment, along with extending the experimental data set, might increase the reliability of the resonant parameters, the S_{11} in particular.

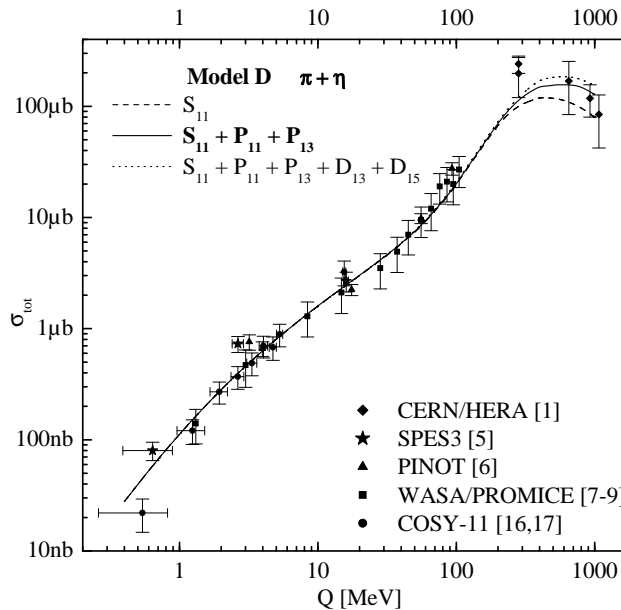


FIG. 5: The total $pp \rightarrow pp\eta$ cross section. In addition to the S-wave, P and D waves are as well used in $xN \rightarrow \eta N$ T -matrices

B. Differential cross sections

We have already determined the ingredients of the model in such a way that the shape and size of the experimental total cross section values are fairly well reproduced. The angular distributions therefore come out as a prediction. Comparing the predictions of model D with the known experimental values of differential cross sections represent an additional test of understanding the physical nature of the process.

Since the final state consists of three particles, one can construct and measure several partially integrated differential cross sections. The $pp\eta$ system in the final state is described by 12 variables and 7 of them are fixed by energy-momentum conservation and particle masses. The differential cross sections with respect to the 5 remaining quantities can be measured. We have compared the predictions of our model with the experimental values for the angular distribution $d\sigma/d\Omega_\eta$, where Θ_η is the angle of the η momentum in the center-of-mass frame with respect to the beam axis, and the invariant mass distribution $d\sigma/ds_{pp}$ where s_{pp} is the proton-proton invariant mass. Measurements of these quantities have been recently reported by Calén [9] at CELSIUS facility for $Q = 15$ and 37 MeV, Moskal [17] at COSY-11 for $Q = 15.5$ MeV, and Abdul-Bary [25] $Q = 16$ and 41 MeV at COSY TOF (time of flight) detector. The Abdul-Bary [25] experiment as well gives the value of $d\sigma/ds_{pp}$ at the $Q = 4.5$ MeV. The differential cross sections with respect to the remaining two variables of interest (proton- η invariant mass and the angle of relative momentum of the proton-proton system to the beam axis) have been mea-

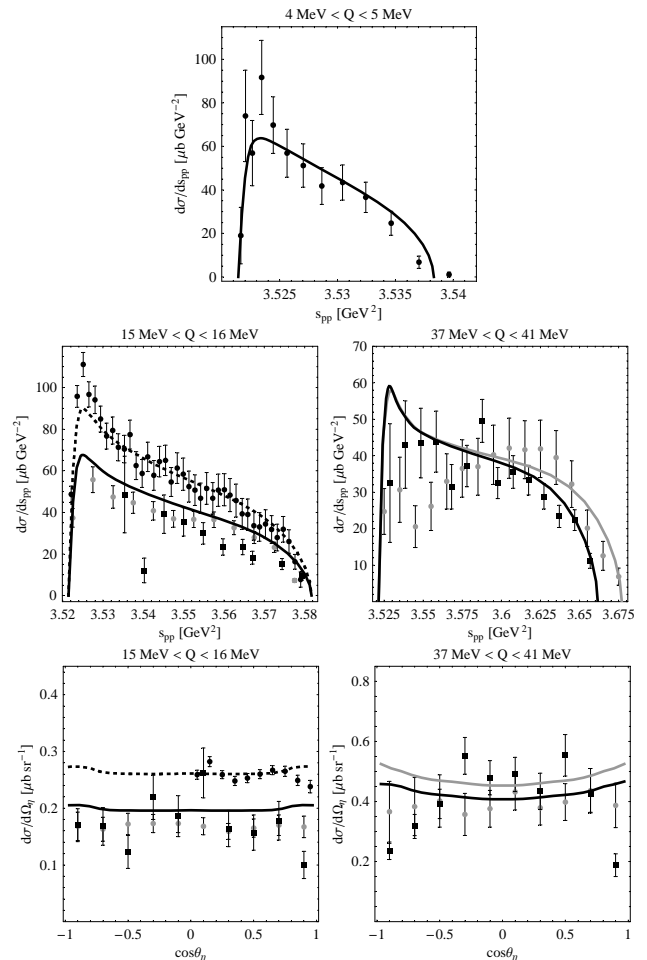


FIG. 6: The differential cross sections. Data are from Calén [9] (black squares), Abdul-Bary [25] (gray circles), and Moskal [17] (black circles). The black full lines are predictions of model D of this article for excess energies 4.5 MeV, 16 MeV, and 37 MeV respectively. The black dashed line is model D prediction for 16 MeV normalized by the factor 1.35. The gray line is model D prediction for 41 MeV.

sured, but are not evaluated in this article. The fifth variable, the azimuthal orientation, is of no significance in the unpolarized measurements.

Before we start the comparison we feel compelled to comment the overall agreement of existing experiments. Out of three experiments, two of them (Calén [9] and Moskal [17]) report quantitative measurements, while the third one (Abdul-Bary [25]) gives results in arbitrary units only, and normalizes to Calén [9]. The two quantitative experiments are clearly in strong disagreement at nearby energies: Calén at $Q = 37$ MeV [9] vs. Abdul-Bary at $Q = 41$ MeV [25]. It is interesting to mention that initially reported values of the COSY-11 experiment [26] are very similar to the Calén [9]. However, in the currently valid version of the measured data the calibration have been increased by $\approx 40\%$ at $Q = 15.5$ MeV, but remained within the error bar for the $Q = 4.5$ MeV

[17]. So, we are left with the situation that we can just compare the shape of differential cross sections paying less importance to the magnitude. Disregarding the absolute normalization we see the fair agreement of the shape of the differential cross section for all experiments at $Q \approx 15$ MeV. At $Q \approx 41$ MeV some discrepancies remain: the Calén [9] data show the distinct structure in $d\sigma/d\Omega_\eta$ which is missing in ref. [25], and the shape of $d\sigma/ds_{pp}$ is notably different in both experiments. However, the differences remain within error bars. It is therefore clear that the detailed quantitative comparison of theory and experiment can not be done and that achieving the quantitative agreement awaits for the experimental accordance.

In Fig. 6 we show the results of our calculations compared to the world data collection. The full lines give the comparison of model D predictions with experiment. The present model nicely reproduces the strong dynamically created departure of both differential cross sections from the symmetric, phase space induced shape. The agreement in shape and size is good for all energies, with the exception of $Q = 15.5$ MeV value of Moskal (COSY-11) [17]. However, if we normalize our model predictions by 35 % (Fig. 6 - dashed line) the data are again reproduced very nicely. For the $d\sigma/ds_{pp}$ the low s_{pp} peaking is nicely followed for all three energies, but the more pronounced structure at $s_{pp} \approx 3.63$ GeV² in the Abdul-Bary data

[25] for $Q = 41$ MeV is not understood. The same agreement in general trend is achieved for the $d\sigma/d\Omega_\eta$ but the Calén structure at $Q = 37$ MeV is not accounted for.

V. SUMMARY

Within the framework of the proposed model we show that the single resonance model, using only N(1535), drastically fails to describe the experimental data. Next S_{11} resonance, N(1650), has to be included in any model to obtain the shape of the total cross section. The inclusion of the third, controversial, N(2090) S_{11} resonance represents a further improvement. The inclusion of P-waves is essential for the energies $100 \text{ MeV} < Q < 1 \text{ GeV}$. All these contributions are effectively incorporated in the proposed model. The FSI corrections are essential to obtain the qualitative and quantitative agreement with experiment. The present way how the FSI is treated in this article, namely using only the S-waves for the Jost function in the low energy effective range approximation, is enough to understand the data to the present level of experimental precision. The improvement of the data, the differential cross sections in particular, will require the improvement of the FSI treatment as well.

-
- [1] E. Flamino *et al.*, CERN-HERA Report 84-01.
 [2] J. F. Germond and C. Wilkin, *Nucl. Phys. A* **518** (1990) 308.
 [3] J. M. Laget and F. Wellers, *Phys. Lett. B* **257** (1991) 254.
 [4] T. Vetter *et al.*, *Phys. Lett. B* **263** (1991) 153.
 [5] A. M. Bergdolt *et al.*, *Phys. Rev. D* **48** (1993) R2969; F. Hibou *et al.*, *Phys. Lett. B* **438** (1998) 41.
 [6] E. Chivassa *et al.*, *Phys. Lett. B* **232** (1994) 270.
 [7] H. Calén *et al.*, *Phys. Lett. B* **365** (1996) 39; H. Calén *et al.*, *Uppsala University preprint TSL/ISV-95-0124* .
 [8] H. Calén *et al.*, *Phys. Rev. C* **58** (1998) 2667.
 [9] H. Calén *et al.*, *Phys. Lett. B* **458** (1999) 190.
 [10] C. Wilkin, *Phys. Rev. C* **47** (1993) R938.
 [11] G. Faeldt *et al.*, *Nucl. Phys. A* **604** (1996) 441.
 [12] A. B. Santra and B. K. Jain, *Nucl. Phys. A* **634** (1998) 309.
 [13] E. Gedalin, A. Moalem and L. Razdolskaja, *Nucl. Phys. A* **634** (1998) 368.
 [14] M. Batinić, A. Švarc and T.-S. H. Lee, *Physica Scripta* **56** (1997) 321.
 [15] M. Batinić, *et al.*, *Phys. Rev. C* **51** (1995) 2310; M. Batinić, *et al.*, *Physica Scripta* **58** (1998) 15.
 [16] J. Smyrski *et al.*, *Phys. Lett. B* **474** (2000) 182.
 [17] P. Moskal, *et al.*, *Phys. Rev. C* **69** (2004) 025203
 [18] K. Nakayama *et al.*, *Phys. Rev. C* **68** (2003) 045201.
 [19] R. Machleidt, *Adv. Nucl. Phys.* **19**, (1989) 189.
 [20] A. König and P. Kroll, *Nucl. Phys. A* **356** (1981) 345.
 [21] M. L. Goldberger and K. M. Watson: *Collision Theory*, John Wiley & Sons, Inc. (1964); U. Schubert, *Acta Universitatis Upsaliensis* **5** (1995); V. Bernard, N. Kaiser, and U.-G. Meißner, *Eur. Phys. J. A* **4** (1999) 259.
 [22] V. G. J. Stoks and Th. A. Rijken, *Phys. Rev. C* **59** (1999) 3009.
 [23] J. R. Bergervoet, *et al.*, *Phys. Rev. C* **38** (1988) 15.
 [24] S. Ceci and A. Švarc, *Few-Body Systems Suppl.* **14** (2003) 311.
 [25] M. Abdul-Bary *et al.*, *Eur. Phys. J. A* **16** (2003) 127.
 [26] P. Moskal *et al.*, *PiN Newslett.* **16** (2002) 367.